Bifunctional TiO_2 (anatase, brookite, rutile)-based photocatalysis for environment remediation: efficient simultaneous glyphosate degradation and H_2 production

Muhammad Umair, Leonardo Palmisano, Marianna Bellardita*

Engineering Department, University of Palermo, Viale delle Scienze Ed. 6, 90128, Palermo, Italy.

*Corresponding author: Marianna Bellardita. E-mail: marianna.bellardita@unipa.it

Abstract

Glyphosate is currently the most widely used herbicide in the world due to its broad-spectrum effectiveness and relatively low cost. However, its massive and prolonged application has raised serious environmental concerns. In this context, novel strategies for the effective degradation of glyphosate and its derivatives are urgently needed. One promising and sustainable approach is the use of the photocatalytic method. In this study, we explore, a polyfunctional photocatalytic system capable of producing high-value compounds by oxidation of glyphosate and simultaneously obtaining H_2, a clean energy carrier. Namely, both organic and inorganic valuable compounds have been obtained by the partial oxidation of glyphosate. The effectiveness of various TiO_2 based commercial and home prepared polycrystalline photocatalysts has been explored. Pt-TiO_2 or Cu_2O-TiO_2 heterostructured samples were also investigated. Preliminary results demonstrated that under UV irradiation, the proposed photocatalyst achieves high glyphosate degradation rates along with appreciable H_2 evolution. The photocatalysts showed stability over repeated cycles and maintained their activity, indicating their practical potential. Mechanistic studies suggest that photogenerated holes were primarily responsible for the oxidative degradation of glyphosate, while photoexcited electrons drove the reduction of protons to H_2 gas. Pt-Brookite, used for the first time in this reaction, resulted in the most active photocatalysts affording about 51% of glyphosate conversion and an H_2 production of 0.34 mM.

Environmental Implication

Photocatalytic systems enabling simultaneous glyphosate degradation and hydrogen production present a dual environmental benefit aligned with the sustainability goals highlighted by the Journal of Hazardous Materials. This approach addresses the persistence and ecotoxicity of glyphosate in aquatic

environments while valorizing it as a sacrificial agent for clean energy generation. By coupling pollutant removal with renewable H_2 production under mild conditions, the process reduces secondary waste, chemical inputs, and energy demand compared to conventional treatments. For these reason we believe that this work is environmentally relevant.

Keywords: Wastewater treatment; Environment remediation; Glyphosate removal; Glyphosate photoreforming; Green H_2 production, Brookite TiO_2.

1. Introduction

Water pollution is one of the major global challenges that human society is facing nowadays. Worldwide, around 2.1 billion people lack access to safe water, which causes millions of deaths every year [1]. The excessive use of herbicides to increase agricultural production has led to the contamination of water, generating serious environmental damage [2, 3]. Glyphosate (N-phosphonomethyl glycine or PMG) is a highly effective broad-spectrum herbicide for weed control, first introduced in 1974 and marketed as Roundup [4]. The use of PMG has increased exponentially over time because it effectively and indiscriminately eradicates weeds, and genetically modified crops resistant to PMG are widely planted with the assumption that the side effects of PMG are negligible [5, 6]. However, on the other hand, its massive use has caused concerns about environmental pollution because only a very small amount of applied PMG is absorbed by crops while its key intermediates, such as its metabolite aminomethylphosphonic acid (AMPA), end up in the environment [7-10]. Biologically, PMG can be degraded in soil by enzymes that act through two main processes. Through the primary degradation pathway that occurs naturally, PMG oxidoreductase cleaves the C-N bond, producing glyoxylate and AMPA [11]. The presence of AMPA makes the C-N pathway less desirable because its greater persistence compared to PMG makes it more toxic to the environment [12]. In the second pathway, which occurs under isolated conditions, PMG C-P lyase catalyzes the cleavage of the C-P bond, forming phosphate and sarcosine [13]. The C-P lyase pathway is preferable because it produces environmentally safe products. For example, sarcosine can be further broken down into glycine and used as growth food by soil microorganisms [14]. The International Agency for Research on Cancer (IARC) has classified PMG as "Category 2a", indicating that this compound is probably carcinogenic to humans [15]. Therefore, there is a need to develop simple, effective, and environmentally friendly methods to degrade PMG into small, non-toxic inorganic molecules.

Heterogeneous photocatalysis has attracted considerable attention as a green and potentially cost-effective technology for wastewater remediation (although there is a lack of practical large-scale applications in this field) [16, 17], production of high added value compounds [18] and of H_2 [19, 20]. Charge separation occurs when a semiconductor is irradiated with light energy equal to or greater than its band gap energy. The degradation of pollutants in water occurs under aerobic conditions, i.e. in the presence of O_2 with the contribution of photogenerated holes that produce reactive species such as hydroxyl ($^{\bullet}OH$), superoxide ($O_2^{\bullet-}$), and hydroperoxide ($HO_2^{\bullet}$) radicals. These latter species can lead to the complete mineralization of the organic pollutants present and/or to their partial oxidation into valuable compounds [17, 21]. On the other hand, photogenerated electrons can enable the formation of H_2 by water splitting or photoreforming in the presence of sacrificial agents (used to minimize the recombination of photoproduced charges) that capture the holes and partially oxidize to form high-value chemicals [22, 23]. The simultaneous degradation of pollutants with H_2 production is like killing two birds with one stone: cleaning up the environment and powering the future by producing clean energy. Few studies have focused on the photocatalytic degradation of PMG [24] and only one, to the best of our knowledge, has investigated its photoreforming [25], whilst, generally, only the conversion of PMG has been evaluated [26].

TiO_2 is an n-type photocatalyst that is widely used due to its properties such as abundance, non-toxicity, high (photo)stability, high oxidizing power and relative cheapness [27]. This solid exists in various polymorphic crystalline phases, the most important of which are anatase, brookite and rutile. Its physicochemical properties and different photocatalytic activity depend on the type of phase (or mixture of phases) under investigation [22].

Anatase is generally the most active polymorph for total oxidation reactions, rutile shows some efficiency in particular reactions, brookite has good performance for H_2 production [19, 22, 28, 29].

However, bare TiO_2 displays low or negligible activity towards H_2 production due to its fast recombination rate of electron and hole pairs, wide band gap (3.2 eV) and conduction band edge potential near to that of H^+ reduction. Studies showed that n-type TiO_2 samples coupled with p-type materials form an effective heterojunction able to improve charge separation and solar light absorption thus enhancing the photoactivity [30]. For example, Cu_2O is a low cost, non-toxic and easily prepared, p-type semiconductor with a band gap of 2.2 eV and conduction band potential more negative than that of the H^+/H_2O pair [31, 32]. The combination of Cu_2O with TiO_2 forms a p-n type heterojunction resulting in absorption into visible region and improves photogenerated charge carrier separation [33-35]. Platinum

(Pt), on the other hand, acts as a co-catalyst attracting the photogenerated electrons thanks to its high work function and capability to extend light absorption towards the visible light region [36, 37].

In this study, we investigated the photoreforming of PMG, i.e., its degradation accompanied by the formation of high-value compounds such as formic and glycolic acids, simultaneously with H_2 production. Pt- or Cu_2O were used as co-catalysts to enhance the performance of TiO_2 based photocatalysts.

Notably, for the first time, to our knowledge, brookite TiO_2 was used for this kind of reaction in addition to other solids consisting of different TiO_2 polymorphs. Some photocatalysts, like the commercial TiO_2 P25, were used only for the sake of comparison as they are known to be particularly photoactive. Inorganic ions such as phosphate and ammonium were also obtained, confirming the degradation of PMG into harmless compounds. Furthermore, with the aim of replacing the noble metal with less expensive non-metallic species, 3%Cu_2O-TiO_2 heterostructured samples were used as the photocatalysts, as they showed in the past high performances for H_2 production [38, 39].

2. Experimental

2.1 Chemicals

Titanium dioxide (TiO_2, P25 Aeroxide), Platinum chloride ($PtCl_4$, BDH chemicals), ethanol (C_3H_5OH, Sigma-Aldrich), hydrochloric acid (HCl, Sigma-Aldrich), titanium tetrachloride ($TiCl_4$, Sigma-Aldrich) copper(I) oxide (Cu_2O, Riedel-de Haën) were used as received without purification.

2.2 Samples preparation

2.2.1 Anatase

Anatase was synthesized by adding $TiOSO_4$ (40 g) to distilled water (180 mL) and stirring for 2 h until a clear suspension was formed. The resulting mixture was transferred to a Pyrex bottle and heated in an oven at 100°C for 48 h. After separating the solid formed by filtration, the latter was washed with double-distilled water to remove the sulfate ions, dried at 60 °C and finally calcined for 3 h at 600 °C.

2.2.2 Brookite

The sample TiO_2 brookite was synthesized by hydrothermal hydrolysis. Typically, distilled water (420 mL), HCl (160 ml), $TiCl_4$ (10 mL) were added to a 1L beaker and stirred for 2h. Then, the resulting mixture was transferred to a Pyrex bottle and heated at 100 °C for 48 h in an oven. The obtained powder

was a mixture of brookite and rutile. The brookite was separated in the supernatant by peptizing with water at different times from the rutile that was present in the precipitates.

2.2.3 Rutile

The sample rutile was prepared by adding $TiCl_4$ (20 mL) to distilled water (100 mL) and stirring for 2 h at room temperature. The resulting mixture was transferred to a Pyrex bottle and heated at 100 ℃ for 48 h in an oven. The rutile powder was obtained after drying in a rotary evaporator at 50 ℃.

2.2.4 Cu_2O-TiO_2 samples

Two different composites were obtained by mixing Cu_2O with TiO_2 P25 or Brookite in a zirconium oxide coated steel jar containing six zirconium oxide balls by using a Retsch Ball Mills, type PM100 milling. The samples were prepared according to previously determined best conditions such as 150 rpm for 2 h and 3%Cu_2O.

2.2.5 Pt loaded samples

TiO_2 P25 was modified with 0.5 wt% Pt by the photodeposition method. Typically, distilled water (400 mL), ethanol (100 mL), $PtCl_4$ (10 mL), and the TiO_2 sample (2 g) were added to the photoreactor. Initially, the mixture was stirred for 30 minutes in dark with He bubbling to eliminate O_2 and then the lamp was turned on under stirring for 7-8 h. After that, mixture was filtered, washed and then dried in an oven for 5-6 h.

2.3 Characterizations

X-ray diffraction (XRD) patterns of the used samples were acquired by a Philips diffractometer (working at current of 30 mA and voltage of 40 kV) using CuKα radiation. The Raman spectra of the tested samples were analyzed by a BWTek-i-micro Raman Plus system connected with a 785 nm diode laser. A Flow Sorb 2300 instrument (Micromeritics) was used to calculate specific surface area (SSA) using the single-point BET technique. A Shimadzu UV-2401 PC spectrophotometer was used to acquire UV–Vis diffuse reflectance spectra (DRS) at room temperature using barium sulphate ($BaSO_4$) as a reference material and the wavelength range was 200–800 nm. The band gap values of the used samples were calculated by plotting the modified Kubelka-Munk function $[F(R'_\infty)hv]^{1/2}$ versus the energy of the exciting light. A Perkin Elmer LS55 fluorescence spectrometer was used to record the photoluminescence (PL) spectra of

the different materials in the 300–600 nm range, with a 300 nm excitation wavelength. A Nova NanoSEM (Scanning Electron Microscopy) equipment was used to examine the morphology of the tested samples. A small quantity of powder samples was put on carbon tape that was fastened to a stub made of stainless steel.

Cationic and anionic species were analyzed using a Dionex ICS-1000 and ICS-1100 ion chromatograph equipped with IONPAC® AS23 and IONPAC® CS16 anion-exchange and cation-exchange columns, respectively. For the cation-exchange column, the mobile phase consisted of a 0.03 mol/L CH_3SO_3H solution, while for the anion-exchange column, it consisted of a mixture of 0.8 mmol/L $NaHCO_3$ and 45 mmol/L Na_2CO_3.

2.4 Photocatalytic activity

The experiments were carried out under anaerobic conditions at natural pH in a cylindrical reactor of 150 mL at room temperature and pressure. The temperature of the reactor was maintained by a Pyrex cooling jacket with water circulation. The initial concentration of PMG was 1 mM and the duration of the experiments was 5 h. Initially, the reactor was filled with PMG solution and catalyst, stirred in dark for 30 minutes with He bubbling to achieve adsorption-desorption equilibrium and to remove the dissolved air. Then, the reaction mixure was illuminated with a UV 125 W medium pressure Hg lamp and every 30 minutes samples were withdrawn. The liquid samples were filtered by 2µm membranes (HA, Millipore) and analyzed in a Thermo Scientific Dionex ultimate 3000 HPLC, equipped with refractive index detectors and a Diode Array. The column used was a Phenomenex REZEK ROA H^+ Organic acid, the eluent 2.5 mM H_2SO_4 aqueous solution and the flow rate 0.6 mL/min. For the determination of gaseous species (H_2 and CO_2), a gas tight syringe of 500 µL was used and analyzed in a HP 6890 Series GC System equipped with a Supelco packed column GC 60/80 Carboxen$^{TM-1000}$ and a thermal conductivity detector (TCD). To identify the main active species involved in the photocatalytic degradation of PMG, runs after adding selected scavengers were carried out in the presence of the most performant photocatalyst. Namely, tert-butanol, $AgNO_3$, $Na_2C_2O_4$ were used as $^{\bullet}OH$, electrons, and holes scavengers, respectively.

3. Results and discussions

Figure 1 shows the XRD patterns of the different samples. The three phases (anatase, brookite and rutile) of TiO_2 are present in the used photocatalysts identified by the characteristic peaks at $2\theta = 25.5°$, 38.0°,

48.0°, 54.5° for anatase, 2θ = 25.34°, 25.69◦, 30.81° for brookite and 2θ = 27.5°, 36.5°, 41°, 54.1° 56.5° for rutile. Anatase and rutile polymorphs coexist in commercial P25, while the pure phases are present in the home-prepared anatase, brookite, and rutile samples. The presence of Pt was not observed due to its low amount and high degree of dispersion on the surface of TiO_2. The 3%Cu_2O-P25 sample, in addition to the characteristic anatase and rutile peaks, presents a small peak at 2θ = 36.2°, confirming the presence of Cu_2O in the TiO_2 matrix. Compared to samples such as Pt-Brookite, 3%Cu_2O-Brookite and Pt-Rutile, the peaks of the P25 and anatase based samples are narrower and more intense, suggesting a larger crystallite size and higher crystallinity (Table 1) which can be explained by their preparation at a higher temperature.

To further study the structure of the samples used, Raman spectra were recorded (Figure 1 (B)). The bands indicated the presence of anatase phase characterized by the main peaks at 144 cm^{-1}, 197 cm^{-1}, 396 cm^{-1}, 514 cm^{-1} , and 637 cm^{-1}, brookite at 126 cm^{-1}, 152 cm^{-1}, 212 cm^{-1}, 247 cm^{-1}, 322 cm^{-1}, 364 cm^{-1}, 409 cm^{-1}, 456 cm^{-1}, 498 cm^{-1}, 543 cm^{-1}, 582 cm^{-1} and 632 cm^{-1} and rutile at 446 cm^{-1} and 613 cm^{-1} [40]. No peaks of foreign species such as Pt or Cu_2O were observed, probably due to low amounts and high degrees of dispersion on the surface of TiO_2.

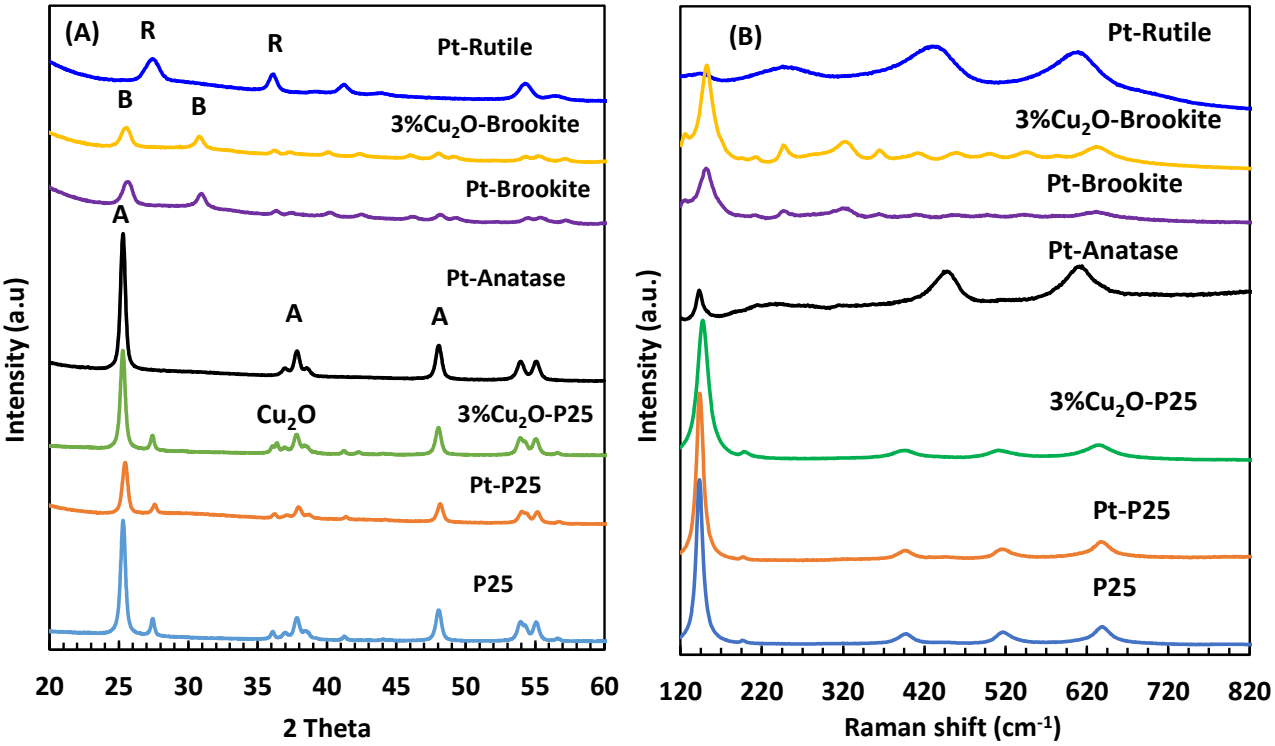

Figure 1. (A) XRD patterns and (B) Raman spectra of different samples used.

P25 showed SSA of 52 m^2 g^{-1} and was almost unchanged after the addition of Pt or Cu_2O. Pt-Brookite, 3%Cu_2O-Brookite and Pt-Rutile showed SSA of 98, 91 and 85 m^2 g^{-1} respectively. Figure 2 (Left-side) shows the UV-Vis DRS spectra of the different samples. All of them are active in the UV-Vis region. P25 shows a transition edge at 360 nm, corresponding to the band gap of anatase that is mainly present while rutile is in low amount. The colour of the samples turned grayish after the addition of platinum and pink after coupling with Cu_2O, and consequently a decrease in reflectance was observed in these samples. Pt-Rutile showed the lowest band gap value (3.02 eV), and its transition edge was shifted towards higher wavelength while Brookite displayed the highest figure, in accordance with literature [41].

PL spectra can be used to determine the tendency of photocatalysts to charge transfer and recombination of photogenerated pairs. A high PL emission intensity indicates a fast rate of electron-hole recombination, which is detrimental to photocatalytic efficiency because it means that fewer charge carriers are available for the desired reaction. Figure 2 (right side) reports the PL spectra of different samples. All samples show peaks at around 420, 475 and 530 nm and the addition of foreign species did not change the shape of the spectra, indicating that they do not give rise to new radiative phenomena but only to an increase in the transfer rate of the photogenerated charges. The main band at approximately 420 nm originates from the transition of electrons from the conduction band to the valence band in TiO_2, and is consistent with the band gap values. The bands at longer wavelengths can instead be attributed to the non-radiative recombination of electrons in some lattice defects [42]. The addition of Pt or Cu_2O caused a decrease in the band intensity, indicating a less significant recombination of the photogenerated electron-hole pairs, and suggesting the occurrence of an increase in photocatalytic performance compared to the corresponding bare samples.

Table 1. TiO_2 phase (A=Anatase, R=Rutile, B= Brookite), specific surface area (SSA) and band-gap (E_g) for the different samples.

Sample	Crystalline phase	SSA ($m^2 \cdot g^{-1}$)	E_g (eV)
P25	A, R	52	3.18
Pt-P25	A, R	50	3.10
Pt-Anatase	A	50	3.26

Pt-Brookite	B	98	3.34
Pt-Rutile	R	85	3.02
3%Cu_2O-P25	A, R	48	3.08
3%Cu_2O-Brookite	B	91	3.32

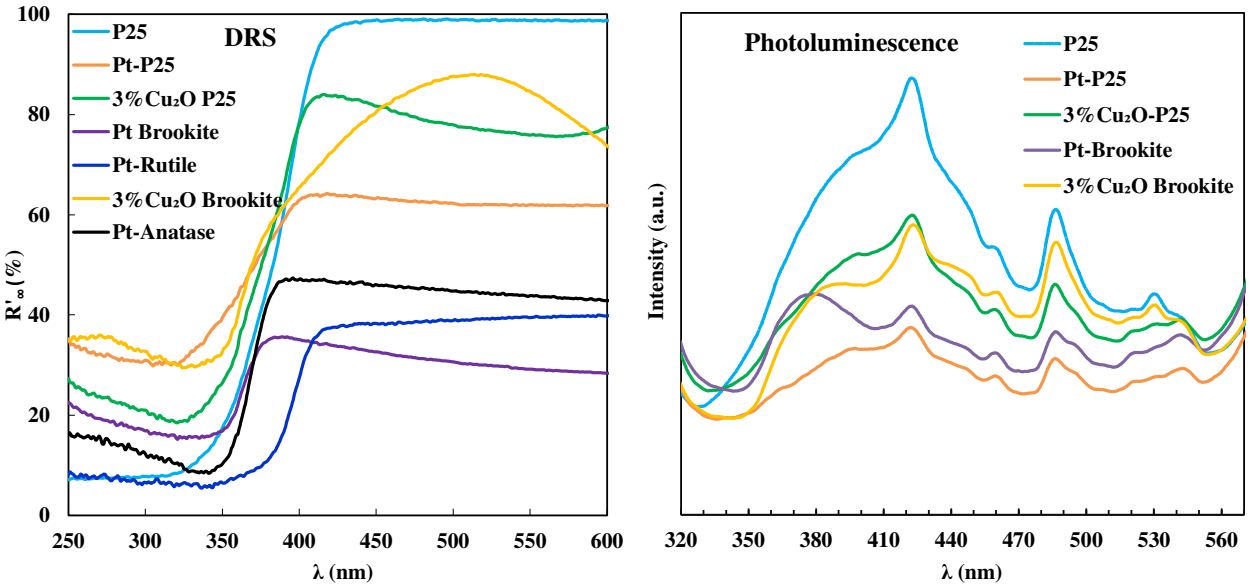

Figure 2. UV-Vis DRS and PL spectra of different samples used.

SEM images were acquired (Figure 3) to study the morphology of the different photocatalysts. All powders showed the presence of aggregates of irregularly shaped particles, whose dimensions ranged from 30 to 140 nm. The presence of foreign species (Pt or Cu_2O) was not observed, likely due to their low loading and homogeneous dispersion within the TiO_2 framework. As a result, the overall morphology closely resembled that of the bare TiO_2 samples. Therefore, the different photoactivities observed (see section 4) are not due to different sample morphologies.

Figure 4 shows TEM images of the Pt–TiO_2 powders. A fairly homogeneous distribution of Pt nanoparticles on the TiO_2 surface can be observed. The Pt particle size is similar in both photocatalysts, with an average diameter of approximately 2–3 nm. Therefore, it is reasonable to assume that the differences in photocatalytic performance observed among the samples are not attributable to variations in Pt particle size.

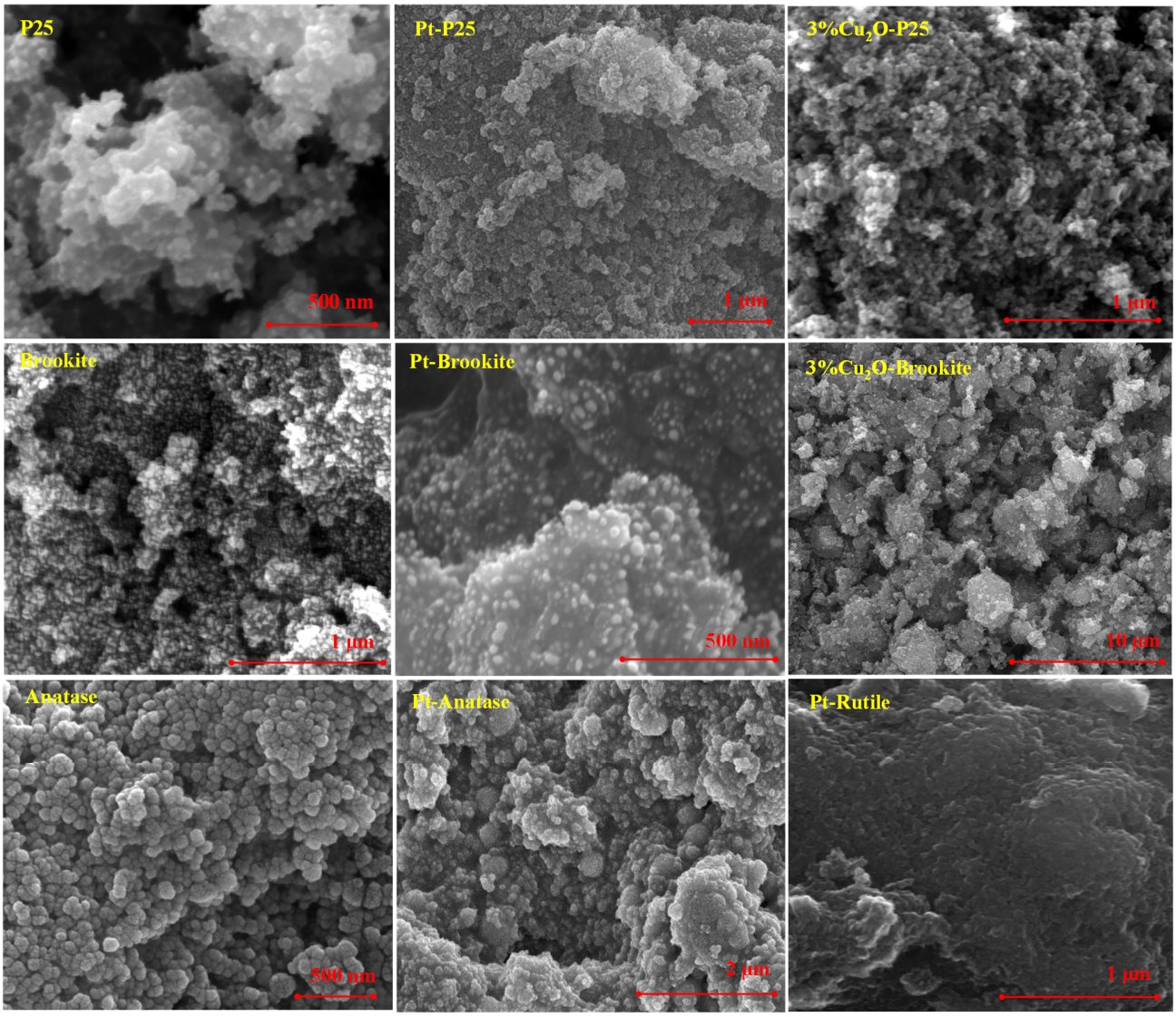

234

235 **Figure 3.** SEM images of different samples used.

236

237

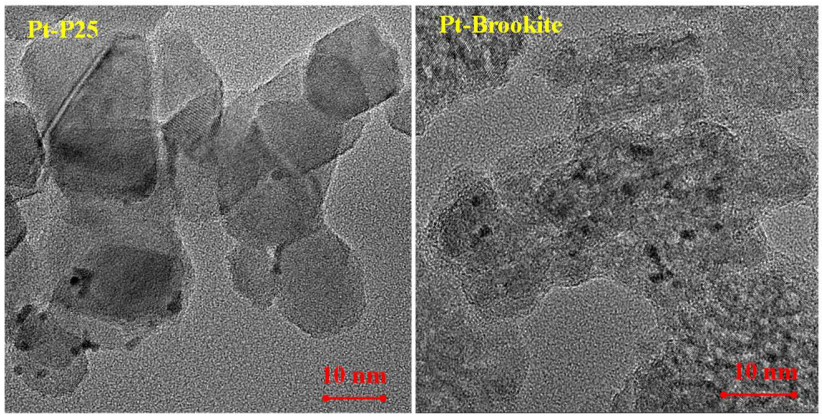

238

Figure 4. TEM images of Pt-P25 and Pt-Brookite photocatalysts.

4. Photocatalytic activity

All TiO_2 based samples were tested under UV irradiation in anaerobic conditions. In this study, we compared commercial P25 and different phases (Anatase, Brookite and Rutile) of home-prepared TiO_2 based photocatalysts modified with Pt or Cu_2O. Conversion (X) and selectivity (S) towards the products were calculated by using the following equations 1 and 2:

$$X = [\frac{C_i - C_t}{C_i}] \times 100 \qquad \text{Equation (1)}$$

$$S = [\frac{P_t}{C_i - C_t}] \times 100 \qquad \text{Equation (2)}$$

where C_i represents the initial PMG molar concentration, C_t shows the molar concentration at any time interval t and P_t is the molar concentration of the product at any time t.

Table 2 shows the results obtained during the degradation of PMG (1 mM), comparing the conversion and the selectivity values towards the main intermediate products in the liquid phase i.e., formic acid and glyoxylic acid over 5 h of irradiation. The amounts of gaseous species (H_2 and CO_2) accumulated in the headspace of the reactor are also reported. No H_2 production was observed in the presence of bare P25 due to poor charge separation and the intrinsic low energetic efficiency of this photocatalyst towards H_2 production [19, 22]. PMG conversion was 14% along with formic acid selectivity of 83% (no glyoxylic acid was observed) and a fair mineralization degree. Pt, due to the higher value of the work function [43, 44] is recognized as the most active metallic co-catalysts for H_2 production, because, acting as an electron sink, enhances the separation of photogenerated electron-hole pairs. For this reason, Pt has been photodeposited on the different photocatalysts. In the presence of Pt-P25, conversion increased 1.78 times compared to bare P25 with selectivity reaching 100 and 35% towards formic acid and glyoxylic acid, respectively. At the same time, the amounts of H_2 and CO_2 produced were 0.11 and 0.009 mM, respectively. To replace Pt with non-metallic species, a 3%Cu_2O-P25 composite was tested, which proved to be very active for glycerol photoreforming even under direct sunlight [38]. The coupling of Cu_2O with TiO_2 proved to be effective for H_2 production also in the case of PMG photoreforming, although the conversion and selectivity values were lower than those obtained in the presence of Pt-P25. However, in

our opinion, these results not only confirm the effectiveness of Cu_2O in replacing noble metals for H_2 production, but also suggest that its behaviour should be further investigated in the future [39].

To investigate whether the home-prepared brookite, which has proven effective for H_2 production, also exhibits activity in this reaction, Pt-loaded brookite was selected as the photocatalyst [22]. Also in this case, this photocatalyst turned out to be the best one, allowing a PMG conversion of 51% and a selectivity towards formic and glyoxylic acids of 100% and 20%, respectively (Figure 4) and with a contemporary maximum H_2 formation of 0.34 mM. The high H_2 production can be ascribed to a synergistic effect between electronic and surface brookite features. The rutile phase (Pt-rutile) showed the lowest activity for PMG conversion and no H_2 production was observed, probably due to the higher recombination of the photoproduced pairs and thermodynamically unfavorable intrinsic electronic properties.

Pt-anatase was more active than Pt-rutile due to the more negative conduction band position of anatase compared to rutile [45], giving a PMG conversion of 28% with H_2 production of 0.15 mM and the selectivities obtained were 73 and 19% for formic and glyoxylic acid, respectively. Brookite, the least common TiO_2 polymorph, exhibits peculiar features as strong redox potential than anatase and rutile [46], higher hydroxylation degree [47] and higher ability to adsorb water [22]. Notably, although the partial oxidation of PMG has been investigated by some authors [24], no quantitative data related to the formed intermediates are reported.

Table 2. Results obtained during photoreforming with glyphosate (1 mM) after 5 hours of UV irradiation using a 125 W medium pressure Hg lamp and bubbling He. X= Conversion; S= Selectivity.

Sample	$X_{Glyphosate}$ (%)	$S_{Formic\ acid}$ (%)	$S_{Glyoxylic\ acid}$ (%)	H_2 [mM]	CO_2 [mM]
P25	14	83	-	0.00	0.0062
Pt-P25	25	100	35	0.11	0.0089
3%Cu_2O-P25	19	82	18	0.14	0.0080
Pt-Brookite	51	100	20	0.34	0.0043
3%Cu_2O-Brookite	28	65	16	0.05	0.0168
Pt-Anatase	28	73	19	0.15	0.0091
Pt-Rutile	9	100	-	0.00	0.0065

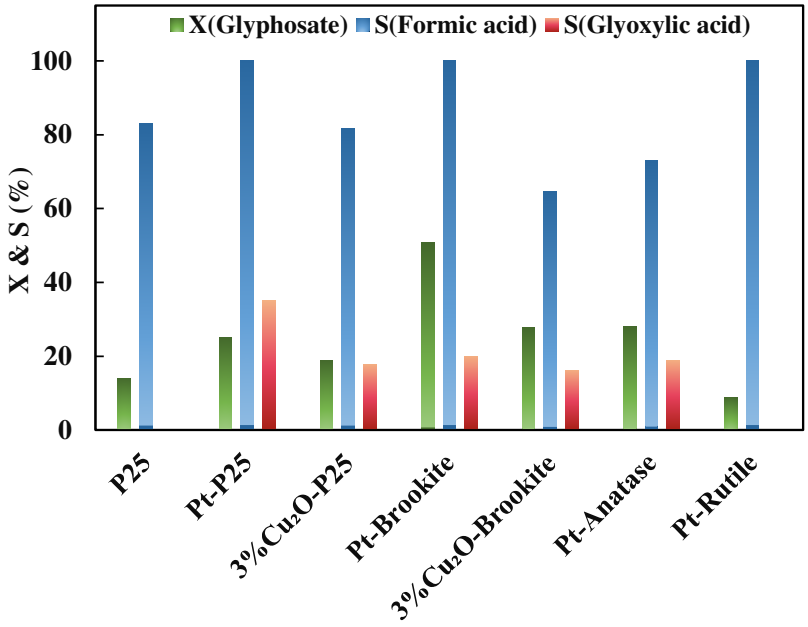

Figure 4. Glyphosate conversion (X) and selectivity (S) towards formic acid and glyoxylic acid in the presence of the different photocatalysts after 5h of irradiation.

The effective cleavage of C–N or C–P bonds in glyphosate (Figure 5) is indicated by the high selectivity towards formic acid, which might have been facilitated by the Pt-based catalysts (highlighted as blue in Table 2). Formic acid and glyoxylic acid are both valuable chemicals with important industrial and commercial applications. For example, formic acid is used as an intermediate in the production of formaldehyde-free resins [48, 49] and as a preservative and antibacterial agent [50]. Glyoxylic acid is used as a reducing agent in the preparation of different chemicals, as an intermediate for glycine (an amino acid used in the food and pharmaceutical industries) preparation [51], in the synthesis of vanillin (used as a flavouring and fragrance chemical) [52], as a starting material for allantoin (used in the cosmetic industry) [53] and as a precursor in the production of imidazoles, oxazoles and other heterocycles [54].

A possible reaction pathway has been hypothesized in Figure 5. PMG undergoes bond cleavage through two probable roots, leading to the formation of high-value intermediates and ultimately to mineralization with the formation of inorganic phosphate, ammonia, and CO_2. In turn, the photoproduced electrons drive the reduction of protons to H_2. Then, the combined process allows environmental remediation transforming glyphosate, its valorization obtaining high added value compounds by partial oxidation and the production of a renewable fuel by the electrons.

Figure 5 schematically illustrates the hypothesized reaction pathways occurring during PMG photoreforming. Cleavage of the C-N bond can lead to the formation of glyoxylic acid, followed by further cleavage to formic acid, and finally mineralization to CO_2, H_2O. In the same time H^+ cleavage gives rise to H_2 by means of electrons. The parallel pathway involving the cleavage of the C-P and C-N bonds produces two ionic species: phosphate and ammonia. Also, these latter can be considered valuable compounds as they find application in the fertilizer industry.

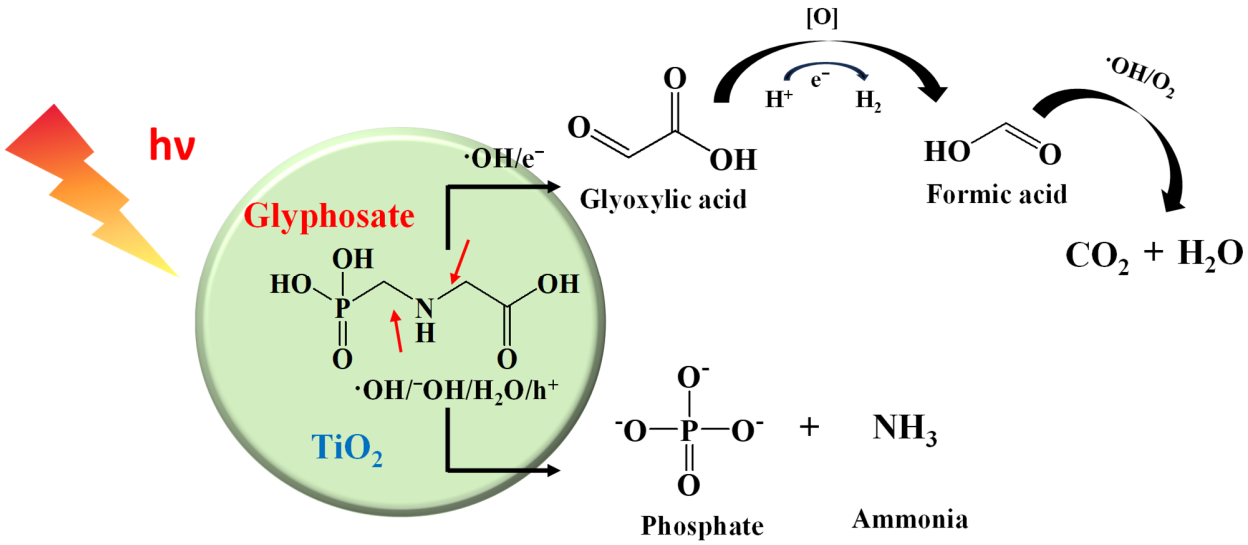

Figure 5. Reaction scheme of glyphosate photoreforming.

In Table 3, phosphate and ammonium concentrations measured by ion chromatography during the photoreforming of PMG in the presence of Pt-Brookite and Pt-P25 are reported. During the photocatalytic reaction a continuous increase in concentration was determined for both species, showing a progressive cleavage of the C–P and C–N bonds present in PMG molecule.

Table 3. Concentrations of phosphate and ammonia in the presence of Pt-Brookite and Pt-P25.

	Pt-Brookite		**Pt-P25**	
	C (mM)		**C (mM)**	
T (min)	**Phosphate**	**Ammonium**	**Phosphate**	**Ammonium**
0	0	0	0	0
120	0.059	0.034	0.086	0.028

240	0.130	0.057	0.150	0.060
300	0.149	0.065	0.231	0.075

The catalyst that proved to be the best, i.e., Pt-Brookite, was tested in the presence of different scavengers to identify the main reactive species involved in PMG degradation (Figure 6A). After the addition of $AgNO_3$, no substantial change in PMG conversion was observed suggesting that electron trapping favours the oxidation reaction enhancing holes transfer to the substrate. On the other hand, the presence of tert-butanol and $Na_2C_2O_4$ significantly reduced the degradation efficiency, indicating that hydroxyl radicals ($^{\bullet}OH$) and holes (h^+), trapped by tert-butanol and $Na_2C_2O_4$, respectively, play an important role. The intermediate activity of the experiment without scavengers, however, suggests that several reactive species synergistically participate in the overall photocatalytic activity of Pt-Brookite. Monitoring the production of H_2 during irradiation (Figure 6B) reveals three key trends. First, adding tert-butanol does not noticeably affect the amount of H_2 formed, indicating that hydroxyl radicals do not play a significant role in the H_2 production pathway. Second, introducing $Na_2C_2O_4$ leads to a slight increase in H_2 production, which can be attributed to the higher availability of electrons after holes scavenging by oxalate. Finally, when $AgNO_3$ is present, no H_2 is produced at all, consistent with the fact that silver ions efficiently scavenge electrons.

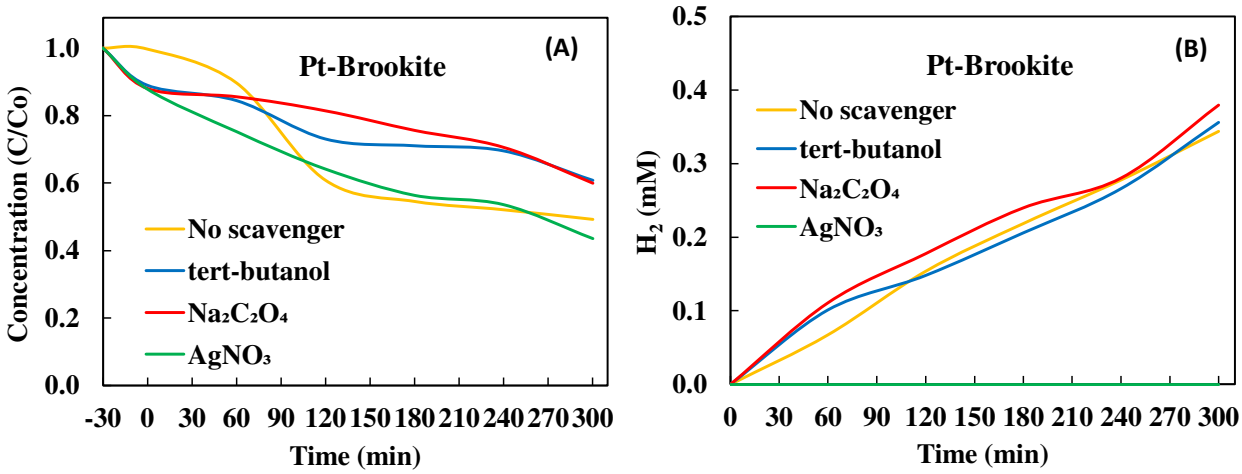

Figure 6. Comparison of PMG degradation (A) and H_2 evolution (B) by using Pt-Brookite in the presence of different scavengers.

In Table 4 the ammonia and phosphate concentrations, in the absence and presence of scavengers, are compared during the irradiation time. After adding tert-butanol and $Na_2C_2O_4$ the concentration of the ionic species is lower than that observed in their absence, confirming the active role of $^{\bullet}OH$ and h^+ in PMG degradation, in accordance with the data reported in Figure 6. Following the addition of $AgNO_3$, the ammonia concentration increases, indicating that trapping of photogenerated electrons suppress the charges recombination, thereby enhancing the oxidation reaction. Conversely, the amount of phosphate decreases with respect to the experiment in the absence of $AgNO_3$, and this result is difficult to rationalize, although a tentative explanation could be the interaction between Ag^+ and phosphate ions producing poorly soluble Ag_3PO_4.

Table 4. Concentrations of phosphate and ammonia in the presence of Pt-Brookite and different scavengers.

	tert-butanol		**$Na_2C_2O_4$**		**$AgNO_3$**	
T (min)	**Phosphate**	**Ammonium**	**Phosphate**	**Ammonium**	**Phosphate**	**Ammonium**
-30	0	0	0	0	0	0
120	0.029	0.058	0.031	0.064	0.025	0.093
240	0.050	0.123	0.055	0.154	0.041	0.171
300	0.063	0.147	0.065	0.005	0.048	0.200

Conclusion

This work investigates glyphosate photoreforming in the presence of selected TiO_2 based photocatalysts with the aim of verifying the feasibility of the process. Namely, the runs were carried out under anaerobic conditions to exploit the possibility of the contemporary oxidation/partial oxidation of PMG and H_2 production. The system successfully achieved this objective by simultaneously addressing three key aspects: (i) environmental remediation through the degradation of glyphosate; (ii) generation of value-added compounds via its partial oxidation; and (iii) concurrent H_2 production. In other words, one process delivers environmental, chemical, and energy benefits simultaneously. Interestingly, TiO_2 Pt-Brookite, used for the first time in this reaction, resulted the most performant photocatalyst, confirming the efficiency of this TiO_2 polymorph in H_2 production. To the best of our knowledge, this study represents one of the first examples in which three objectives are achieved simultaneously, establishing a new paradigm in environmental remediation that integrates contaminant degradation with energy generation

and chemicals production. This approach opens new opportunities for the design of multifunctional photocatalysts tailored to specific pollutants degradation/valorization. In conclusion, future developments of this preliminary work should focus on the exploration of novel photocatalysts and on the integration of suitable separation systems with the reactor to enable the efficient recovery of the value-added chemicals produced.

Acknowledgements

The authors thanks SiciliAn MicronanOTecH Research And Innovation Center "SAMOTHRACE" (MUR, PNRR-M4C2, ECS_00000022), spoke 3 - Università degli Studi di Palermo "S2-COMMs - Micro and Nanotechnologies for Smart & Sustainable Communities" for financial support.

References

[1] N. Pichel, M. Vivar, M. Fuentes, The problem of drinking water access: A review of disinfection technologies with an emphasis on solar treatment methods, Chemosphere 218 (2019) 1014–1030. https://doi.org/10.1016/j.chemosphere.2018.11.205.

[2] W. Zhou, M. Li, V. Achal, 2025. A comprehensive review on environmental and human health impacts of chemical pesticide usage. Emerg. Contam. 11, 100410. https://doi.org/10.1016/j.emcon.2024.100410.

[3] A. Parven, I.M. Meftaul, K. Venkateswarlu, M. Megharaj, Herbicides in modern sustainable agriculture: environmental fate, ecological implications, and human health concerns, Int. J. Environ. Sci. Technol. 22 (2025) 1181–1202. https://doi.org/10.1007/s13762-024-05818-y.

[4] S.O. Duke, S.B. Powles, Glyphosate: a once-in-a-century herbicide, Pest Manag. Sci. 64 (2008) 319–325. https://doi.org/10.1002/ps.1518.

[5] R. Annett, H.R. Habibi, A. Hontela, Impact of glyphosate and glyphosate-based herbicides on the freshwater environment, J. Appl. Toxicol. 34 (2014) 458–479. https://doi.org/10.1002/jat.2997.

[6] L. Cao, D. Ma, Z. Zhou, C. Xu, C. Cao, P. Zhao, Q. Huang, Efficient photocatalytic degradation of herbicide glyphosate in water by magnetically separable and recyclable

395 $BiOBr/Fe_3O_4$ nanocomposites under visible light irradiation, Chem. Eng. J. 368 (2019) 212–
396 222. https://doi.org/10.1016/j.cej.2019.02.100.
397 [7] V.C. Aparicio, E. De Gerónimo, D. Marino, J. Primost, P. Carriquiriborde, J.L. Costa,
398 Environmental fate of glyphosate and aminomethylphosphonic acid in surface waters and soil
399 of agricultural basins, Chemosphere 93 (2013) 1866–1873.
400 https://doi.org/10.1016/j.chemosphere.2013.06.041.
401 [8] O.K. Borggaard, A.L. Gimsing, Fate of glyphosate in soil and the possibility of leaching to
402 ground and surface waters: a review, Pest Manag. Sci. 64 (2008) 441–456.
403 https://doi.org/10.1002/ps.1512.
404 [9] S. Singh, V. Kumar, S. Datta, A.B. Wani, D.S. Dhanjal, R. Romero, J. Singh, Glyphosate
405 uptake, translocation, resistance emergence in crops, analytical monitoring, toxicity and
406 degradation: a review, Environ. Chem. Lett. 18 (2020) 663–702.
407 https://doi.org/10.1007/s10311-020-0
408 [10] S. Singh, V. Kumar, J.P.K. Gill, S. Datta, S. Singh, V. Dhaka, D. Kapoor, A.B. Wani, D.S.
409 Dhanjal, M. Kumar, et al., Herbicide glyphosate: toxicity and microbial degradation, Int. J.
410 Environ. Res. Public Health 17 (2020) 7519. https://doi.org/10.3390/ijerph17207519.
411 [11] H. Zhan, Y. Feng, X. Fan, S. Chen, Recent advances in glyphosate biodegradation, Appl.
412 Microbiol. Biotechnol. 102 (2018) 5033–5043. https://doi.org/10.1007/s00253-018-9035-0.
413 [12] M. Sun, H. Li, D.P. Jaisi, Degradation of glyphosate and bioavailability of phosphorus
414 derived from glyphosate in a soil-water system, Water Res. 163 (2019) 114840.
415 https://doi.org/10.1016/j.watres.2019.07.007.
416 [13] C.A. Villamar-Ayala, J.V. Carrera-Cevallos, R. Vasquez-Medrano, P.J. Espinoza-
417 Montero, Fate, eco-toxicological characteristics, and treatment processes applied to water
418 polluted with glyphosate: a critical review, Crit. Rev. Environ. Sci. Technol. 49 (2019) 1476–
419 1514. https://doi.org/10.1080/10643389.2019.1579627.
420 [14] Y. Huang, Z. Li, K. Yao, C. Chen, C. Deng, Y. Fang, R. Li, H. Tian, Suppressing toxic
421 intermediates during photocatalytic degradation of glyphosate by controlling adsorption
422 modes, Appl. Catal. B: Environ. 299 (2021) 120671.
423 https://doi.org/10.1016/j.apcatb.2021.120671.
424 [15] IARC Working Group on the Evaluation of Carcinogenic Risks to Humans, Some
425 organophosphate insecticides and herbicides, International Agency for Research on Cancer,
426 Lyon, France, 2017.

[16] R. Molinari, F. Pirillo, V. Loddo, L. Palmisano, Heterogeneous photocatalytic degradation of pharmaceuticals in water by using polycrystalline TiO_2 and a nanofiltration membrane reactor, Catal. Today 118 (2006) 205–213. https://doi.org/10.1016/j.cattod.2005.11.091.

[17] U.I. Gaya, A.H. Abdullah, Heterogeneous photocatalytic degradation of organic contaminants over titanium dioxide: a review of fundamentals, progress and problems, J. Photochem. Photobiol. C: Photochem. Rev. 9 (2008) 1–12. https://doi.org/10.1016/j.jphotochemrev.2007.12.003.

[18] G. Palmisano, V. Augugliaro, M. Pagliaro, L. Palmisano, Photocatalysis: a promising route for 21st century organic chemistry, Chem. Commun. (2007) 3425–3437. https://doi.org/10.1039/B700395C.

[19] M. Bellardita, E.I. García-López, G. Marcì, L. Palmisano, Photocatalytic formation of H_2 and value-added chemicals in aqueous glucose (Pt)-TiO_2 suspension, Int. J. Hydrogen Energy 41 (2016) 5934–5947. https://doi.org/10.1016/j.ijhydene.2016.02.103.

[20] J. Du, S. Ma, H. Liu, H. Fu, L. Li, Z. Li, Y. Li, J. Zhou, Uncovering the mechanism of novel $AgInS_2$ nanosheets/TiO_2 nanobelts composites for photocatalytic remediation of combined pollution, Appl. Catal. B: Environ. 259 (2019) 118062. https://doi.org/10.1016/j.apcatb.2019.118062.

[21] M. Bellardita, V. Loddo, L. Palmisano, Formation of high added value chemicals by photocatalytic treatment of biomass, Mini-Rev. Org. Chem. 17 (2020) 884–901. https://doi.org/10.2174/1570193X17666200131112856.

[22] C.M. Pecoraro, L. Mino, E. Kozyr, L. Palmisano, F. di Franco, V. Loddo, M. Santamaria, M. Bellardita, Pt–TiO_2 catalysts for glycerol photoreforming: comparison of anatase, brookite and rutile polymorphs, Chem. Commun. 60 (2024) 3782–3785. https://doi.org/10.1039/D4CC00353E.

[23] M.O. Segovia-Guzmán, M. Román-Aguirre, J.Y. Verde-Gomez, V.H. Collins-Martínez, G. Zaragoza-Galán, V.H. Ramos-Sánchez, Green Cu_2O/TiO_2 heterojunction for glycerol photoreforming, Catal. Today 349 (2020) 88–97. https://doi.org/10.1016/j.cattod.2018.05.031.

[24] Q.Y. Tang, M.J. Yang, S.Y. Yang, Y.H. Xu, Enhanced photocatalytic degradation of glyphosate over 2D CoS/BiOBr heterojunctions under visible light irradiation, J. Hazard. Mater. 407 (2021) 124798. https://doi.org/10.1016/j.jhazmat.2020.124798.

[25] E.N. Musa, S. Kaur, T.C. Gallagher, T.M. Anthony, W.F. Stickle, L. Arnadottir, K.C. Stylianou, Two birds, one stone: coupling hydrogen production with herbicide degradation

over metal–organic framework-derived titanium dioxide, ACS Catal. 13 (2023) 3710–3722. https://doi.org/10.1021/acscatal.3c00265.

[26] F. de J. Silerio-Vázquez, M. García-Roig, L.A. González-Burciaga, C.M. Nunez-Nunez, J.B. Proal-Nájera, Glyphosate photocatalytic degradation: exploring trends, innovations and research gaps, J. Water Process Eng. 66 (2024) 105948. https://doi.org/10.1016/j.jwpe.2024.105948.

[27] A. Patsoura, D.I. Kondarides, X.E. Verykios, Enhancement of photoinduced hydrogen production from irradiated Pt/TiO_2 suspensions with simultaneous degradation of azo-dyes, Appl. Catal. B: Environ. 64 (2006) 171–179. https://doi.org/10.1016/j.apcatb.2005.11.015.

[28] N.S. Allen, N. Mahdjoub, V. Vishnyakov, P.J. Kelly, R.J. Kriek, The effect of crystalline phase (anatase, brookite and rutile) and size on the photocatalytic activity of calcined polymorphic titanium dioxide (TiO_2), Polym. Degrad. Stab. 150 (2018) 31–36. https://doi.org/10.1016/j.polymdegradstab.2018.02.008.

[29] D.R. Eddy, M.D. Permana, L.K. Sakti, G.A.N. Sheha, H. Solihudin, S. Hidayat, T. Takei, N. Kumada, I. Rahayu, Heterophase polymorph of TiO_2 (anatase, rutile, brookite, TiO_2(B)) for efficient photocatalyst: fabrication and activity, Nanomaterials 13 (2023) 704. https://doi.org/10.3390/nano13040704.

[30] Y. Li, B. Wang, S. Liu, X. Duan, Z. Hu, Synthesis and characterization of Cu_2O/TiO_2 photocatalysts for H_2 evolution from aqueous solution with different scavengers, Appl. Surf. Sci. 324 (2015) 736–744. https://doi.org/10.1016/j.apsusc.2014.11.027.

[31] J.-L. Chen, M.-M. Liu, S.-Y. Xie, L.-J. Yue, F.-L. Gong, K.-M. Chai, Y.-H. Zhang, Cu_2O-loaded TiO_2 heterojunction composites for enhanced photocatalytic H_2 production, J. Mol. Struct. 1247 (2022) 131294. https://doi.org/10.1016/j.molstruc.2021.131294.

[32] G. Li, J. Huang, J. Chen, Z. Deng, Q. Huang, Z. Liu, W. Guo, R. Cao, Highly active photocatalyst of Cu_2O/TiO_2 octahedron for hydrogen generation, ACS Omega 4 (2019) 3392–3397. https://doi.org/10.1021/acsomega.8b03404.

[33] Z. Xi, C. Li, L. Zhang, M. Xing, J. Zhang, Synergistic effect of Cu_2O/TiO_2 heterostructure nanoparticle and its high H_2 evolution activity, Int. J. Hydrogen Energy 39 (2014) 6345–6353. https://doi.org/10.1016/j.ijhydene.2014.01.209.

[34] H. Xu, S. Ouyang, D. Wang, J. Ye, L. Liu, T. Kako, Porous-structured Cu_2O/TiO_2 nanojunction material toward efficient CO_2 photoreduction, Nanotechnology 25 (2014) 165402. https://doi.org/10.1088/0957-4484/25/16/165402.

[35] Y.-H. Zhang, M.-M. Liu, J.-L. Chen, K.-F. Xie, S.-M. Fang, Dendritic branching Z-scheme Cu_2O/TiO_2 heterostructure photocatalysts for boosting H_2 production, J. Phys. Chem. Solids 152 (2021) 109948. https://doi.org/10.1016/j.jpcs.2021.109948.

[36] M. Abdennouri, A. Elhalil, M. Farnane, H. Tounsadi, F.Z. Mahjoubi, R. Elmoubarki, M. Sadiq, L. Khamar, A. Galadi, M. Baâlala, M. Bensitel, Photocatalytic degradation of 2,4-D and 2,4-DP herbicides on Pt/TiO_2 nanoparticles, J. Saudi Chem. Soc. 19 (2015) 485–493. https://doi.org/10.1016/j.jscs.2015.06.007.

[37] C.R. López, M.N. Suárez Rodríguez, J.M. Doña Rodríguez, J.A. Navío Santos, D. Fernández Hevia, E. Pulido Melián, J.A. Ortega Méndez, Ó. González-Díaz, Hydrogen production using Pt-loaded TiO_2 photocatalysts, Int. J. Hydrogen Energy (2013). https://doi.org/10.1016/j.ijhydene.2013.07.006.

[38] M. Umair, A. Ruiz-Aguirre, I. Berruti, S. Malato Rodriguez, L. Palmisano, V. Loddo, M. Bellardita, Biomass derivatives photoreforming in pilot plant scale to obtain H_2 under green conditions by using ball milling Cu_2O-TiO_2 P25 photocatalysts, Chem. Eng. J. 504 (2025) 158585. https://doi.org/10.1016/j.cej.2024.158585.

[39] M. Umair, G. Palmisano, R. Al Sakkaf, S. Al Jitan, A. Pintar, G. Žerjav, L. Palmisano, V. Loddo, M. Bellardita, Pt-Nb_2O_5-TiO_2 based semiconductors for photo-reforming of glucose and fructose aqueous solutions, Appl. Surf. Sci. 648 (2024) 159030. https://doi.org/10.1016/j.apsusc.2023.159030.

[40] U.G.E.N. Balachandran, N.G. Eror, Raman spectra of titanium dioxide, J. Solid State Chem. 42 (1982) 276–282. https://doi.org/10.1016/0022-4596(82)90006-8.

[41] A. Di Paola, G. Cufalo, M. Addamo, M. Bellardita, R. Campostrini, M. Ischia, R. Ceccato, L. Palmisano, Photocatalytic activity of nanocrystalline TiO_2 (brookite, rutile and brookite-based) powders prepared by thermohydrolysis of $TiCl_4$ in aqueous chloride solutions, Colloids Surf. A: Physicochem. Eng. Asp. 317 (2008) 366–376. https://doi.org/10.1016/j.colsurfa.2007.11.005.

[42] J. Liqiang, Y. Qu, B. Wang, S. Li, B. Jiang, L. Yang, W. Fu, H. Fu, J. Sun, Review of photoluminescence performance of nano-sized semiconductor materials and its relationships with photocatalytic activity, Sol. Energy Mater. Sol. Cells 90 (2006) 1773–1787. https://doi.org/10.1016/j.solmat.2005.11.007.

[43] M. Bellardita, H.A. El Nazer, V. Loddo, F. Parrino, A.M. Venezia, L. Palmisano, Photoactivity under visible light of metal loaded TiO_2 catalysts prepared by low frequency

ultrasound treatment, Catal. Today 284 (2017) 92–99. https://doi.org/10.1016/j.cattod.2016.11.026.

[44] H.B. Michaelson, The work function of the elements and its periodicity, J. Appl. Phys. 48 (1977) 4729–4733. https://doi.org/10.1063/1.323539.

[45] A. Di Paola, M. Bellardita, R. Ceccato, L. Palmisano, F. Parrino, Highly active photocatalytic TiO_2 powders obtained by thermohydrolysis of $TiCl_4$ in water, J. Phys. Chem. C 113 (2009) 15166–15174. https://doi.org/10.1021/jp904673e.

[46] J. Buckeridge, K.T. Butler, C.R.A. Catlow, A.J. Logsdail, D.O. Scanlon, S.A. Shevlin, S.M. Woodley, A.A. Sokol, A. Walsh, Polymorph engineering of TiO_2: demonstrating how absolute reference potentials are determined by local coordination, Chem. Mater. 27 (2015) 3844–3851. https://doi.org/10.1021/acs.chemmater.5b00230.

[47] M. Bellardita, V. Augugliaro, V. Loddo, B. Megna, G. Palmisano, L. Palmisano, M.A. Puma, Selective oxidation of phenol and benzoic acid in water via home-prepared TiO_2 photocatalysts: distribution of hydroxylation products, Appl. Catal. A: Gen. 441 (2012) 79–89. https://doi.org/10.1016/j.apcata.2012.07.019.

[48] J. Chrobak, J. Iłowska, A. Chrobok, Formaldehyde-free resins for the wood-based panel industry: alternatives to formaldehyde and novel hardeners, Molecules 27 (2022) 4862. https://doi.org/10.3390/molecules27154862.

[49] P. Solt, J. Konnerth, W. Gindl-Altmutter, W. Kantner, J. Moser, R. Mitter, H.W.G. van Herwijnen, Technological performance of formaldehyde-free adhesive alternatives for particleboard industry, Int. J. Adhes. Adhes. 94 (2019) 99–131. https://doi.org/10.1016/j.ijadhadh.2019.04.007.

[50] A. Álvarez, A. Bansode, A. Urakawa, A.V. Bavykina, T.A. Wezendonk, M. Makkee, J. Gascon, F. Kapteijn, Challenges in the greener production of formates/formic acid, methanol, and DME by heterogeneously catalyzed CO_2 hydrogenation processes, Chem. Rev. 117 (2017) 9804–9838. https://doi.org/10.1021/acs.chemrev.7b00159.

[51] D.R. Jarois, L.E. Schimmelpfennig, S.H. Gellman, A new mechanism for formation of glycine from glyoxylic acid: the Aza-Cannizzaro reaction, Chem.–Eur. J. 30 (2024) e202403202. https://doi.org/10.1002/chem.202403202.

[52] P. D'Arrigo, L.A.M. Rossato, A. Strini, S. Serra, From waste to value: recent insights into producing vanillin from lignin, Molecules 29 (2024) 442. https://doi.org/10.3390/molecules29020442.

[53] L. Liu, A. He, X. Li, Synthesis of allantoin catalyzed by SO_4^{2-}/La_2O_3-SiO_2-ZrO_2, Asian J. Chem. 24 (2012) 2298.

[54] J. Sisko, A.J. Kassick, M. Mellinger, J.J. Filan, A. Allen, M.A. Olsen, An investigation of imidazole and oxazole syntheses using aryl-substituted TosMIC reagents, J. Org. Chem. 65 (2000) 1516–1524. https://doi.org/10.1021/jo9917821.